Measurements of In-Plane Material Properties with Scanning Probe Microscopy

Robert W. Carpick and Mark A. Eriksson

Abstract

Scanning probe microscopy (SPM) was originally conceived as a method for measuring atomic-scale surface topography. Over the last two decades, it has blossomed into an array of techniques that can be used to obtain a rich variety of information about nanoscale material properties. With the exception of friction measurements, these techniques have traditionally depended on tip–sample interactions directed normal to the sample's surface. Recently, researchers have explored several effects arising from interactions parallel to surfaces, usually by deliberately applying a modulated lateral displacement. In fact, some parallel motion is ubiquitous to cantilever-based SPM, due to the tilt of the cantilever. Recent studies, performed in contact, noncontact, and intermittent-contact modes, provide new insights into properties such as structural anisotropy, lateral interactions with surface features, nanoscale shear stress and contact mechanics, and in-plane energy dissipation. The understanding gained from interpreting this behavior has consequences for all cantilever-based scanning probe microscopies.

Keywords: *atomic force spectroscopy, mechanical properties, nanomechanics, scanning probe microscopy.*

Introduction

Atomic force microscopy (AFM) refers to techniques that use a force-sensing probe to measure surface properties. Typically, AFM cantilevers are designed to be extremely sensitive to forces normal to the sample surface, and they enable a user to determine properties such as topography with high resolution. Lateral, or friction, force microscopy (LFM/FFM)[1,2] is a modification of AFM that involves measuring the interaction force *parallel* to the sample surface; recent advances in FFM research are reviewed by Perry in this issue of *MRS Bulletin*. One of the most important consequences of the development of FFM is the emergence of the field of nanotribology (see the May 1993 and June 1998 issues of *MRS Bulletin*), from which new, fundamental insights into the origins of friction continue to be uncovered.[3]

In addition to FFM, a range of other distinct methods has been developed in which lateral motion of the tip is used. These in-plane methods span the entire range of AFM techniques, from contact to intermittent- and noncontact regimes, and are applicable to a wide range of materials including thin organic films, ceramics, and metals. This article is motivated by a recent burst of results in the area of in-plane material properties. Examples include lateral stiffness measurements, which are related to the contact area and shear modulus of the materials; intermittent-contact phase measurements, where in-plane structure and dissipation are measured; and noncontact lateral modulation to determine interaction forces in the plane of the sample between the AFM tip and adsorbates or surface features. The emergence of in-plane techniques is highlighted not only by this research, but also by the fact that lateral modulation recently has become available as an operational mode in commercial atomic force microscopes.

Instrumentation Considerations

The precise method of obtaining in-plane measurements depends on the mode of interaction (e.g., the so-called contact, intermittent contact, and noncontact modes), the particular property under examination (structure, friction, elasticity, viscoelasticity), and the type of probe used. Microfabricated cantilevers are most popular, but quartz tuning forks are often used for dynamic measurements, and tapered fibers are used in near-field scanning optical microscopy. The control and quantitative interpretation of these modes require an understanding of the static and dynamic properties of the probe as well of as the entire instrument, not to mention characterization of the tip. Despite the fact that several tip characterization and lever calibration techniques have been described in the literature (e.g., References 4–6), they have yet to be widely adopted and are not easily accessible in commercial AFM systems. Thus, researchers must take care in implementing these methods to obtain quantitative results.

Of particular concern for AFM cantilever probes is the fact that the cantilevers are typically tilted by an angle of 10–20° to ensure that the tip itself makes contact with the sample before any other part, such as the edge of the chip that the lever is attached to. Thus, the bending displacement of the cantilever normal to its plane is *not* normal to the sample's surface plane. It involves a small but significant in-plane displacement in the longitudinal direction (i.e., parallel to the surface, in the plane containing the long axis of the cantilever). This "unintentional" in-plane displacement has measurable effects that are not usually taken into account. Viewed one way, these may be undesirable—for example, if one seeks a purely normal interaction to quantitatively measure topography, adhesion, or mechanical properties. However, these effects can also be used to extract quantitative in-plane information about materials of interest, as will be presented here.

Lateral Stiffness Measurements and Lateral Modulation of the Tip in Contact

Friction in solid–solid nanocontacts below the wear threshold has been observed to be proportional to the true contact area (i.e., the number of interfacial atoms).[3] In other words, friction F_f for a single-asperity contact is given by:

$$F_f = \tau A\,, \tag{1}$$

where A is the contact area and τ is the interfacial shear strength, which corresponds to the friction force per unit area or per interfacial atom. Surprisingly, continuum mechanics often provides an accurate description of the nanometer-scale contact area. There are a range of models that describe A, depending on the nature of the adhesive and elastic properties of the materials.[7–11] The shear strength is not necessarily constant and may be more generally described as a constant plus a pressure-dependent term:

$$\tau = \tau_0 + \alpha P, \tag{2}$$

where P is the nominal contact pressure and α is a dimensionless coefficient; more complex dependencies are certainly possible. The magnitude and pressure dependence of the shear strength will depend on the materials and the sliding conditions (environment and temperature), so determining the shear strength is a key goal in nanotribology—as is the determination of the general validity of Equation 1, which may break down for sufficiently small contacts due to the atomistic scale of the interface.

Contact stiffness is the amount of force per unit displacement required to compress an elastic contact in a particular direction, and it is essentially the "spring constant" of the contact. Contact stiffness applies to both normal and lateral displacements. The lateral contact stiffness, $k_{contact}$, between homogeneous, isotropic, linear elastic materials is directly proportional to the contact radius a, given by:[12]

$$k_{contact} = 8G^*a\,, \tag{3a}$$

where

$$G^* = [(2 - \nu_{tip})/G_{tip} + (2 - \nu_{sample})/G_{sample}]^{-1}. \tag{3b}$$

Here, G and ν are the shear modulus and the Poisson ratio, respectively. This convenient relationship holds for all types of adhesive regimes (which is *not* true for normal stiffness). However, it requires that no interfacial slip occurs; thus, applied lateral forces must be low, and friction must be sufficiently high, to prevent slip. This no-slip condition can be readily achieved for moderate-to-high friction interfaces, or with sufficiently large loads applied. The contact stiffness is in series with the lateral stiffnesses of the cantilever and the tip structure,[13] so the three stiffnesses must be deconvolved. Fortunately, for many commercial cantilevers these instrumental stiffnesses do not dominate the measurement,[4] and thus, commercial cantilevers can be used for these in-plane studies.

The slope of the initial "sticking" portion of the tip–sample interaction during lateral deformation corresponds to the total lateral stiffness of the system, and the contact stiffness is determined by subtracting out the tip and cantilever stiffness. To measure this accurately, the lateral displacement between the cantilever base and the sample is modulated with a small amplitude; thus, the cantilever will exhibit an oscillating twist. A lock-in amplifier measures the lateral force response. A shear piezo under the sample is highly effective for this purpose.[14] Measuring $k_{contact}$ can be viewed in two ways: if the shear modulus is known, then measurement is a means of determining the contact area. If the contact area is known or can be modeled, the measurement gives the nanoscale shear modulus.

Lateral modulation was first demonstrated qualitatively for imaging purposes[15] and then later quantified in terms of contact stiffness.[13,16,17] For example, the variation of total lateral stiffness with load was measured for a SiN_x tip and a muscovite mica sample in ultrahigh vacuum (upper set of symbols in Figure 1a).[18] A substantial variation is observed, due to the change in contact area with load. Friction can also be measured (lower set of symbols in Figure 1a). The continuum adhesive contact area model by Johnson, Kendall, and Roberts[8] fits both sets of data well. However, one can determine the load dependence of τ without relying on any contact area model by simply dividing friction at each load by the square of the corresponding contact stiffness. Using Equations 1 and 3a, we find:

$$\frac{F_f}{k_{contact}^2} = \frac{\pi\tau}{64(G^*)^2} \propto \tau, \tag{4}$$

so the ratio $F_f/k_{contact}^2$ is proportional to τ. This result is plotted in Figure 1b, from which it can be seen that the shear strength is load-independent, demonstrating that over this pressure range, friction increases with load simply due to the increase in the real contact area. However, the friction force *per unit area*, or *per atom* (the shear strength), remains constant, and the mechanism of frictional dissipation is unchanged. Lateral stiffness measurements have been applied to a range of other material pairs and environments, including silicon nitride tips on muscovite mica samples in air;[16] Si tips on $NbSe_2$ samples in UHV;[16] and silicon tips on silicon oxide, mica, carbon fibers, and epoxy samples in air and vacuum,[19] revealing that the pressure dependence of the shear strengths depends on both the material studied and the environment used.

Lateral modulation of the tip in contact reveals other properties, such as viscoelastic and rheological response, as demonstrated successfully in the case of viscoelastic contacts by examining the time and phase lag between the lateral drive and the sample's response while varying the load.[20] In addition, lateral modulation methods have been used to study glass transitions,[21] friction dynamics, and nanoscale rheology in polymers and liquids.[22–24] Other variations enable simultaneous and higher-speed detection of shear deformation and friction using in-plane modulation.[25–27]

Materials with In-Plane Anisotropy

Materials are often anisotropic, and this anisotropy can be manifested in the surface plane. In-plane anisotropy has been revealed via friction imaging due to several effects, ranging from in-plane aligned polymerization[28] and tilt angle in monolayers[29–32] to in-plane orientation of polar molecular groups in ferroelectrics.[33]

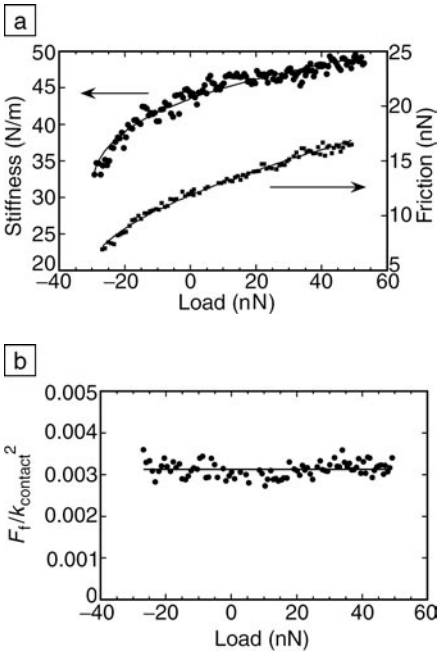

Figure 1. (a) Upper symbols: total lateral stiffness versus load data for a SiN_x tip on muscovite mica in ultrahigh vacuum. Lower symbols: friction versus load for the same system. Curves are fits of the JKR (Johnson, Kendall, and Roberts) adhesive contact model to both measurements. (b) Ratio of the friction force to the square of the contact stiffness, $F_f/k_{contact}^2$, versus load. This is calculated from the stiffness and friction data in (a), as shown in Equation 4. This quantity is proportional to the shear strength and shows that it is independent of load in this range.

Polydiacetylene (PDA) is a particularly interesting material to consider from the standpoint of anisotropy. PDA thin films are prepared by Langmuir[34] or self-assembly techniques.[35] The structure discussed here, illustrated in Figure 2b, consists of a single molecular layer of hydrocarbon chains linked together by polymer backbones running parallel to the surface. The backbones are highly linear and aligned. Friction measurements (Figure 2c) reveal a domain structure.[28] Friction varies substantially from one domain to the next, but it is uniform within each domain. The large-scale topographic image (Figure 2a) reveals a flat film, athough higher-resolution topographic images within a single domain reveal parallel striations of varying width (Figure 2d). These striations are associated with the direction of the underlying backbone. Friction is lowest when sliding occurs parallel to the backbones, and it is nearly three times larger when sliding occurs perpendicular to them. This dramatic effect may be due to anisotropic packing and/or ordering of the hydrocarbon side chains, as well as the anisotropic stiffness of the polymer backbone itself.

Most investigations of in-plane anisotropy have relied on contact-mode friction imaging. One recent exception is a new form of SPM that uses a near-field scanning optical microscope (NSOM) probe (essentially a tapered optical fiber) to image the anisotropy of PDA. Distance regulation in a NSOM is often carried out by oscillating the tip laterally near, but not in contact with, the surface—the so-called shear-force damping method. By adapting the method to allow lateral oscillation in any in-plane direction, shear-force damping can be used to study in-plane anisotropy.[36]

Imaging In-Plane Anisotropy with IC-AFM

The high in-plane anisotropy of PDA films provides an opportunity to reexamine common assumptions about SPM techniques, including intermittent-contact AFM (IC-AFM), often referred to as tapping-mode or "amplitude-controlled" dynamic AFM.[37,38] In IC-AFM, the cantilever is driven at or near its resonant frequency. The tip interacts strongly with the sample for only a small portion of its cycle, and the resulting reduced amplitude is used as a feedback signal to map the sample's topography. The phase shift between the drive and response is monitored simultaneously and is generally considered to be a map of dissipation during compression of the sample along the sample normal, although there are many contributions to this phase shift.

Figure 3 shows an IC-AFM topographic image of a PDA monolayer (Figure 3a), along with a phase image (Figure 3b) that reveals the in-plane structure of this molecular monolayer as well as phase contrast due to the in-plane orientation of the polymer backbones.[37] Given that the properties of PDA films normal to the substrate are highly uniform for all domains, this clearly

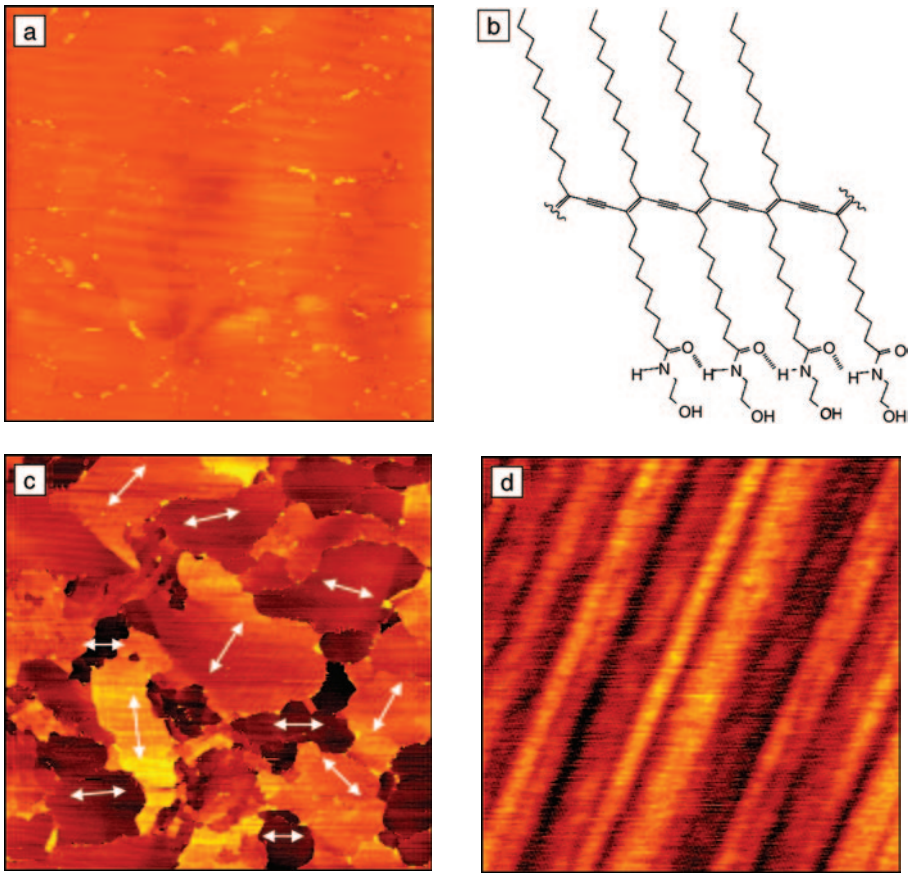

Figure 2. (a) 50 μm × 50 μm AFM topography image of a polydiacetylene (PDA) monolayer. (b) Structure of the PDA monolayer, consisting of hydrocarbon chains linked by linear polymer backbones parallel to the substrate and aligned with each other. (c) 50 μm × 50 μm simultaneous friction image, revealing the different domains. White arrows indicate the domain orientation. (d) A separate 500 nm × 500 nm topography image of a single domain. The ~2 Å striations are indicative of the backbone orientation.

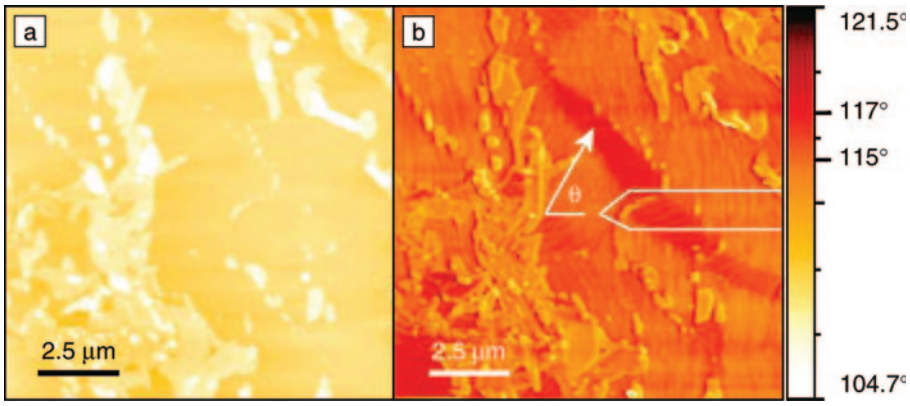

Figure 3. (a) Topographic and (b) phase images of a polydiacetylene (PDA) monolayer thin film on mica. θ is the angle between the local PDA backbone striations and the long axis of the cantilever. The orientation of the cantilever is sketched in (b). The graded color scale indicates the range of phase angles in (b).

shows the influence of in-plane structure due to the tilt of the cantilever. As with contact-mode friction images, PDA domains can be identified in the phase image by the orientation of the striations along which the PDA backbones lie.[34] A darker strip runs diagonally across the phase image, indicative of a net phase difference in that region of approximately 2°. This change in phase is correlated with a change in angle θ between the polymer backbones (as determined from the orientation of the striations) and the long axis of the cantilever. This phase variation is a direct measure of the in-plane properties of the monolayer film.

Phase shifts in IC-AFM indicate energy loss. When the tip motion is sinusoidal, the power dissipated can be calculated from the reduced amplitude and phase.[39,40] As with many IC-AFM measurements, the tip motion is very nearly sinusoidal in these experiments.[37] From Figure 3b and the methods presented in References 39 and 40, the power dissipated is smallest when the striations are parallel to the long axis of the cantilever (as projected onto the sample). In these experiments, the cantilever loses extra energy, $\Delta E \approx 2.4$ eV, per cycle. The phase shift observed in the diagonal dark stripe in Figure 3b can be explained by considering the cantilever's tilt (11° in our case) creating a small but significant component of tip motion parallel to the sample during each cycle. The direction of larger dissipation corresponds with the direction of high friction. The amount of extra energy dissipated is roughly 10% of the total dissipated through the tip–sample interaction. That this level of energy loss should occur is reasonable, given that the in-plane displacement of the tip is ~20% of its total displacement.

IC-AFM Phase Variations as a Function of Cantilever Tilt Angle

The observation of in-plane properties with IC-AFM points to the general importance of cantilever tilt. Recently, we have directly measured the variation of IC-AFM phase as a function of cantilever tilt angle.[41] By mounting Si(111) samples on small wedges, relative tilt angles of 6°, 11°, 16°, and 21° were achieved (see Figure 4a). Figure 4b shows the measured phase shifts as a function of the tilt angle. The experimental parameters are listed in Reference 41. The data exhibit a trend toward 90°, with the phase angle decreasing from approximately 135° to near 105° with increasing positive tilt. Up to a 15° change in phase occurring for a 15° change in lever–sample tilt is observed. In four runs of the same mand laser alignments), the results show the same trend. The offsets in the data sets can be quantitatively accounted for by changes in the tip radius or work of adhesion, both of which commonly vary in AFM experiments. Extrapolating the data back to a sample tilt of –11°, corresponding to "ideal" tip oscillation along the sample normal (0° relative angle), we expect significant in-plane contributions to typical IC-AFM phase data. The trend toward 90° indicates an increase in lateral damping with tilt, because increased damping broadens the phase resonance curve (see inset in Figure 4).

In IC-AFM, there are two modes of stable interaction: either the tip is always entirely within the attractive regime during its oscillation cycle, or the tip encounters intermittent repulsive forces.[42] For Figure 4, the absolute value of the phase is above 90°. As shown by Garcia and San Paulo, this corresponds to the attractive regime only.[42] This is an interesting result: the phase changes significantly as a function of tilt angle due to the in-plane interaction with the sample, even though the tip never encounters a strong repulsive interaction with it.

It is instructive to model the interaction and calculate IC-AFM phase angles as a function of the tilt angle. We assume a

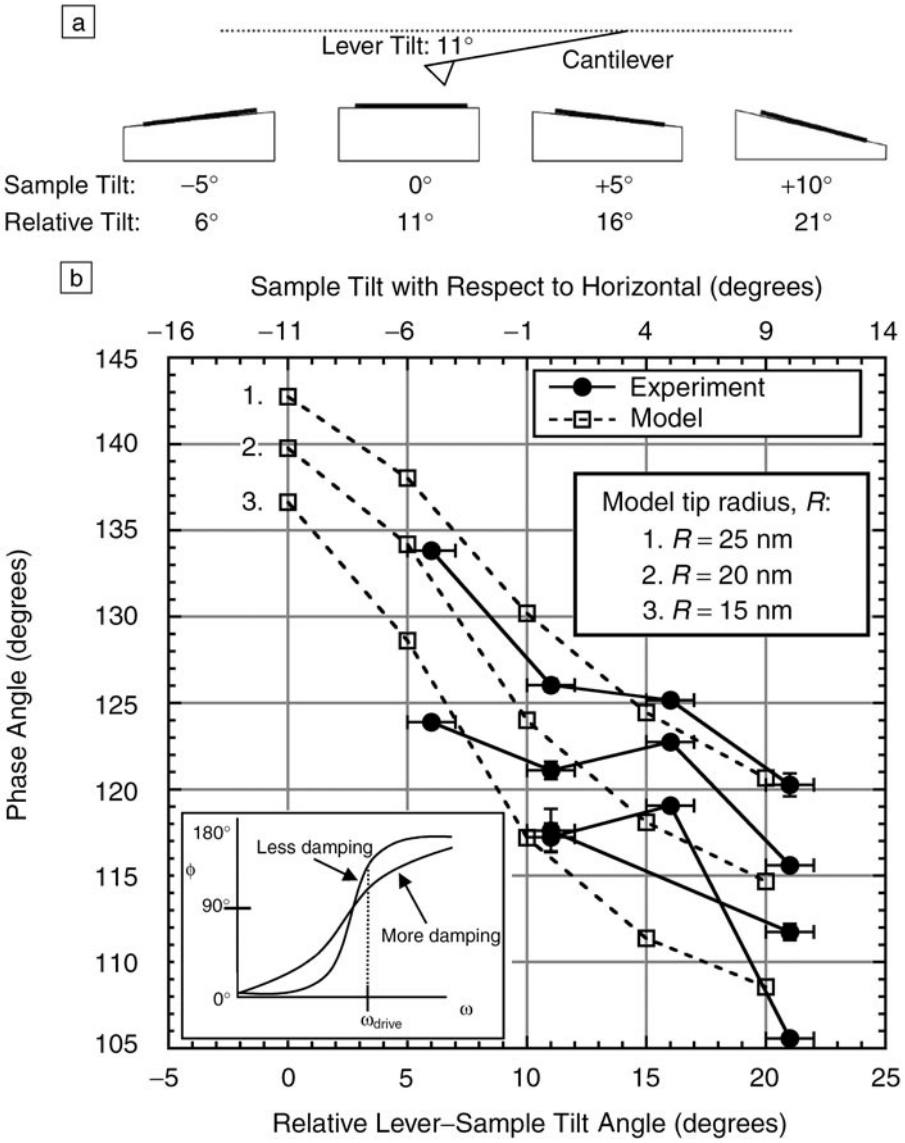

Figure 4. (a) Geometry of the cantilever and the tilted samples. (b) Intermittent-contact AFM phase as a function of cantilever–sample tilt angle. Four sets of experimental data and three sets of results from our model[41] are shown. Horizontal error bars of ±1° are reported, to account for error in alignment of the wedges. The three model curves correspond to the three possible tip radii, as shown in the legend. The inset shows how increased damping shifts the phase toward 90°.

sinusoidally driven, damped harmonic oscillator with damping forces resolved into in-plane and normal components with respect to the surface. Out of contact, the interaction arises from the van der Waals force. We also include a viscous damping layer immediately above the surface that contributes to normal and lateral damping. This model correctly accounts for the experimentally observed phase shifts in Figure 4 with appropriately chosen normal and lateral damping factors. Only the lateral damping term affects the phase shift when the tilt angle is changed, and to match our data, the damping must be surprisingly strong. Clearly, the tilt between the tip and sample leads to measurable phase changes. This means that quantitative interpretation of phase data in IC-AFM requires consideration of the surface slope and the lateral damping characteristics of the surface and near-surface regions.

Noncontact Measurements Using Lateral Modulation

Recently, noncontact dynamic force microscopy was performed by Pfeiffer et al. in an in-plane mode by exciting the high-frequency torsional resonance of a cantilever.[43] The excitation of the fundamental torsional resonance enabled detection of lateral forces in the piconewton range. The experiment was performed in ultrahigh vacuum on a Cu(100) single crystal. The tip height was controlled using a tunneling current as the topographic feedback signal. The surface possessed steps and sulfur impurities, which both show up as doubled features in the frequency shift image due to the lateral oscillation, which was ~2 nm in amplitude (Figure 5). Line traces of the image data show that while the sulfur impurity is not apparent in the topography signal, it clearly appears in the lateral frequency shift. The frequency shift can be converted to a lateral force by an inversion scheme, and the result shows that the tip detects an increased attraction when close to the sulfur impurity and to the step. An additional attraction of the tip toward the step when approaching from the lower terrace is also observed and is due to the enhanced effective area of interaction. This demonstrates that in-plane noncontact AFM can be used as an extremely sensitive probe of surface features. In addition, it has been known for years that lateral and mechanical interactions can be used to activate or induce the motion of atoms, molecules, and nanostructures along surfaces using scanning tunneling microscopy,[44] but the actual forces involved have not been characterized. This technique may now allow these forces to be explored and characterized quantitatively.

Summary and Future Directions

The work reviewed here highlights the wide range of lateral interactions that can be measured with scanning probe microscopy techniques. These interactions reveal new insights into phenomena such as friction, elasticity and viscoelasticity, surface structure, and energy dissipation. The results also show the importance of properly modeling and characterizing the technique at hand, since lateral displacement of the tip can lead to significant features in SPM images.

Continued research is needed to optimize lateral measurement techniques. An example toward this end is a newly developed cantilever that is optimized for lateral force sensitivity.[45] With appropriate effort devoted to quantitative, calibrated methods, a wider range of samples and properties can be investigated. Ultimately, an emphasis on in-plane interactions should lead to a more complete approach to the nanoscale characterization of materials, in which structure, dynamics, and interaction forces can be accurately measured in all three dimensions.

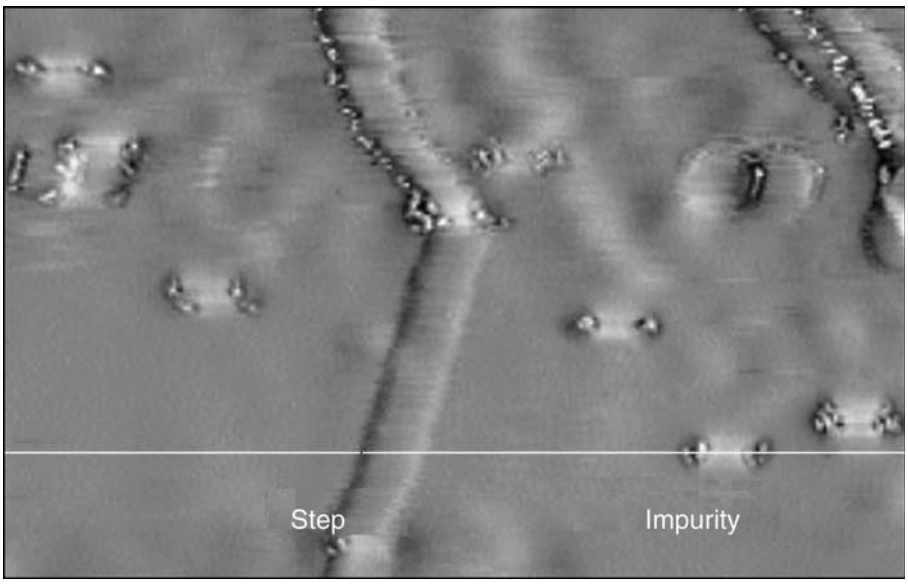

Figure 5. Frequency shift map of the lateral oscillation recorded while scanning at constant tunneling current on a Cu(100) surface (full range, 3.5 Hz). A monatomic step running from top to bottom and several sulfur impurities appear twofold due to the lateral tip oscillation. An oscillation amplitude of 2 nm can be deduced. Image width is 65 nm. (From Reference 43.)

Acknowledgments

We acknowledge funding from the NSF CAREER program, grants DMR0094063 (Eriksson) and CMS0134571 (Carpick); the Research Corporation (Eriksson); the NSF MRSEC program, grant DMR0079983 (Carpick and Eriksson); and the Army Research Office, grant DAAD19-03-1-0102 (Carpick and Eriksson). We thank our colleagues at the University of Wisconsin–Madison, especially Matthew S. Marcus and Matthew J. D'Amato, and Alan R. Burns and Darryl Y. Sasaki at Sandia National Laboratories.

References

1. G. Meyer and N. Amer, *Appl. Phys. Lett.* **57** (1990) p. 2089.
2. S. Alexander, L. Hellemans, O. Marti, J. Schneir, V. Elings, P.K. Hansma, M. Longmire, and J. Gurley, *J. Appl. Phys.* **65** (1989) p. 164.
3. R.W. Carpick and M. Salmeron, *Chem. Rev.* **97** (1997) p. 1163.
4. D.F. Ogletree, R.W. Carpick, and M. Salmeron, *Rev. Sci. Instrum.* **67** (1996) p. 3298.
5. J.E. Sader, J.W.M. Chon, and P. Mulvaney, *Rev. Sci. Instrum.* **70** (1999) p. 3967.
6. J.S. Villarrubia, *J. Res. Natl. Inst. Stand. Technol. (USA)* **102** (1997) p. 425.
7. H. Hertz, *J. Reine Angew. Math.* **92** (1881) p. 156.
8. K.L. Johnson, K. Kendall, and A.D. Roberts, *Proc. R. Soc. London, Series A* **324** (1971) p. 301.
9. B.V. Derjaguin, V.M. Muller, and Y.P. Toporov, *J. Colloid Interface Sci.* **53** (1975) p. 314.
10. D. Maugis, *J. Colloid Interface Sci.* **150** (1992) p. 243.
11. R.W. Carpick, D.F. Ogletree, and M. Salmeron, *J. Colloid Interface Sci.* **211** (1999) p. 395.
12. K.L. Johnson, *Contact Mechanics* (Cambridge University Press, Cambridge, UK, 1987).
13. M.A. Lantz, S.J. O'Shea, A.C.F. Hoole, and M.E. Welland, *Appl. Phys. Lett.* **70** (1997) p. 970.
14. O. Piétrement, J.L. Beaudoin, and M. Troyon, *Trib. Lett.* **7** (2000) p. 213.
15. K. Yamanaka and E. Tomita, *Jpn. J. Appl. Phys., Part 1* **34** (1995) p. 2879.
16. R.W. Carpick, D.F. Ogletree, and M. Salmeron, *Appl. Phys. Lett.* **70** (1997) p. 1548.
17. M.A. Lantz, S.J. O'Shea, M.E. Welland, and K.L. Johnson, *Phys. Rev. B* **55** (1997) p. 10776.

18. R.W. Carpick, M. Enachescu, D.F. Ogletree, and M. Salmeron, in *Fracture and Ductile vs. Brittle Behavior—Theory, Modelling and Experiment*, edited by G.E. Beltz, R.L. Blumberg Selinger, K.-S. Kim, and M.P. Marder (Mater. Res. Soc. Symp. Proc. **539**, Warrendale, PA, 1999) p. 93.
19. O. Pietrement and M. Troyon, *Langmuir* **17** (2001) p. 6540.
20. K.J. Wahl, S.V. Stepnowski, and W.N. Unertl, *Trib. Lett.* **5** (1998) p. 103.
21. Y. Pu, M. Rafailovich, K. Sokolov, Y. Duan, E. Pearce, V. Zaitsev, S. Schwarz, and S. Ge, *Langmuir* **17** (2001) p. 5865.
22. S. Sills and R.M. Overney, *Phys. Rev. Lett.* **91** 095501 (2003).
23. M. He, A.S. Blum, G. Overney, and R.M. Overney, *Phys. Rev. Lett.* **88** 154302 (2002).
24. T. Gray, C. Buenviaje, R.M. Overney, S.A. Jenekhe, L. Zheng, and A.K.Y. Jen, *Appl. Phys. Lett.* **83** (2003) p. 2563.
25. H.-U. Krotil, T. Stifter, and O. Marti, *Appl. Phys. Lett.* **77** (2000) p. 3857.
26. T. Drobek, R.W. Stark, and W.M. Heckl, *Phys. Rev. B* **64** 045401 (2001).
27. K. Yamanaka, A. Noguchi, T. Tsuji, T. Koike, and T. Goto, *Surf. Interface. Anal.* **27** (1999) p. 600.
28. R.W. Carpick, D.Y. Sasaki, and A.R. Burns, *Trib. Lett.* **7** (1999) p. 79.
29. R.M. Overney, H. Takano, M. Fujihira, W. Paulus, and H. Ringsdorf, *Phys. Rev. Lett.* **72** (1994) p. 3546.
30. M. Liley, D. Gourdon, D. Stamou, U. Meseth, T.M. Fischer, C. Lautz, H. Stahlberg, H. Vogel, N.A. Burnham, and C. Duschl, *Science* **280** (1998) p. 273.
31. U. Gehlert, J.Y. Fang, and C.M. Knobler, *J. Phys. Chem. B* **102** (1998) p. 2614.
32. K. Hisada and C.M. Knobler, *Colloids Surf., A* **198-200** (2002) p. 21.
33. H. Bluhm, U.D. Schwarz, K.P. Meyer, and R. Wiesendanger, *Appl. Phys. A* **61** (1995) p. 525.
34. D.Y. Sasaki, R.W. Carpick, and A.R. Burns, *J. Colloid Interface Sci.* **229** (2000) p. 490.
35. M.D. Mowery and C.E. Evans, *Tetrahedron Lett.* **38** (1997) p. 11.
36. A.R. Burns and R.W. Carpick, *Appl. Phys. Lett.* **78** (2001) p. 317.
37. M.S. Marcus, R.W. Carpick, D.Y. Sasaki, and M.A. Eriksson, *Phys. Rev. Lett.* **88** 226103 (2002).
38. M.S. Marcus, M.A. Eriksson, D.Y. Sasaki, and R.W. Carpick, *Ultramicroscopy* **97** (2003) p. 145.
39. J.P. Cleveland, B. Anczykowski, A.E. Schmid, and V.B. Elings, *Appl. Phys. Lett.* **72** (1998) p. 2613.
40. J. Tamayo and R. Garcia, *Appl. Phys. Lett.* **71** (1997) p. 2394.
41. M.J. D'Amato, M.S. Marcus, D.Y. Sasaki, M.A. Eriksson, and R.W. Carpick, *Appl. Phys. Lett.* (2004) in press.
42. R. Garcia and A. San Paulo, *Phys. Rev. B* **60** (1999) p. 4961.
43. O. Pfeiffer, R. Bennewitz, A. Baratoff, E. Meyer, and P. Grütter, *Phys. Rev. B* **65** 161403 (2002).
44. M.F. Crommie, C.P. Lutz, and D.M. Eigler, *Science* **262** (1993) p. 218
45. S.P. Jarvis, H. Yamada, K. Kobayashi, A. Toda, and H. Tokumoto, *Appl. Surf. Sci.* **157** (2000) p. 314. □